

# JGR Atmospheres



## RESEARCH ARTICLE

10.1029/2023JD039789

### Key Points:

- We characterize the variability of monthly mean winds in the mesosphere and lower thermosphere (MLT) over 17 years at Rothera using meteor radar observations and the eXtended version of the Whole Atmosphere Community Climate Model (WACCM-X)
- WACCM-X displays biases in the wintertime winds in the upper MLT. Observed winds are eastwards whilst WACCM-X winds are westwards
- Significant variability, trends and intermittent correlations with the solar cycle, Quasi-Biennial Oscillation and Southern Annular Mode are found in the observed and modeled winds

### Supporting Information:

Supporting Information may be found in the online version of this article.

### Correspondence to:

P. E. Noble,  
pn399@bath.ac.uk

### Citation:

Noble, P. E., Hindley, N. P., Wright, C. J., Cullens, C., England, S., Pedatella, N., et al. (2024). Interannual variability of winds in the Antarctic mesosphere and lower thermosphere over Rothera (67°S, 68°W) during 2005–2021 in meteor radar observations and WACCM-X. *Journal of Geophysical Research: Atmospheres*, 129, e2023JD039789. <https://doi.org/10.1029/2023JD039789>

Received 8 AUG 2023

Accepted 8 FEB 2024









### Author Contributions:

**Conceptualization:** Phoebe E. Noble, Corwin J. Wright, Chihoko Cullens, Scott England, Nicholas J. Mitchell, Tracy Moffat-Griffin

**Data curation:** Phoebe E. Noble, Neil P. Hindley, Chihoko Cullens, Nicholas Pedatella

**Formal analysis:** Phoebe E. Noble, Chihoko Cullens, Scott England

## Interannual Variability of Winds in the Antarctic Mesosphere and Lower Thermosphere Over Rothera (67°S, 68°W) During 2005–2021 in Meteor Radar Observations and WACCM-X

Phoebe E. Noble<sup>1,2</sup> , Neil P. Hindley<sup>1</sup> , Corwin J. Wright<sup>1</sup> , Chihoko Cullens<sup>3</sup> , Scott England<sup>4</sup> , Nicholas Pedatella<sup>5</sup> , Nicholas J. Mitchell<sup>1,2</sup> , and Tracy Moffat-Griffin<sup>2</sup> 

<sup>1</sup>Centre for Climate Adaptation & Environment Research, Department of Electronic Engineering, University of Bath, Bath, UK, <sup>2</sup>Atmosphere, Ice and Climate Team, British Antarctic Survey, Cambridge, UK, <sup>3</sup>Laboratory for Atmospheric and Space Physics, University of Colorado, Boulder, CO, USA, <sup>4</sup>Virginia Polytechnic Institute and State University, Blacksburg, VA, USA, <sup>5</sup>High Altitude Observatory, National Center for Atmospheric Research, Boulder, CO, USA

**Abstract** The mesosphere and lower thermosphere (MLT) plays a critical role in linking the middle and upper atmosphere. However, many General Circulation Models do not model the MLT and those that do remain poorly constrained. We use long-term meteor radar observations (2005–2021) from Rothera (67°S, 68°W) on the Antarctic Peninsula to evaluate the Whole Atmosphere Community Climate Model with thermosphere-ionosphere eXtension (WACCM-X) and investigate interannual variability. We find some significant differences between WACCM-X and observations. In particular, at upper heights, observations reveal eastwards wintertime (April–September) winds, whereas the model predicts westwards winds. In summer (October–March), the observed winds are northwards but predictions are southwards. Both the model and observations reveal significant interannual variability. We characterize the trend and the correlation between the winds and key phenomena: (a) the 11-year solar cycle, (b) El Niño Southern Oscillation, (c) Quasi-Biennial Oscillation and (d) Southern Annular Mode using a linear regression method. Observations of the zonal wind show significant changes with time. The summertime westwards wind near 80 km is weakening by up to 4–5 ms<sup>-1</sup> per decade, whilst the eastward wintertime winds around 85–95 km are strengthening at by around 7 ms<sup>-1</sup> per decade. We find that at some times of year there are significant correlations between the phenomena and the observed/modeled winds. The significance of this work lies in quantifying the biases in a leading General Circulation Model and demonstrating notable interannual variability in both modeled and observed winds.

**Plain Language Summary** The mesosphere and lower thermosphere (MLT), at heights of 80–100 km is an important region for the coupling of the middle and upper atmosphere. We carry out a study of the winds above Rothera (Antarctic Peninsula) for the years 2005–2021. We use observations from a meteor radar which measures winds at heights of 80–100 km and compare with the eXtended version of the Whole Atmosphere Community Climate Model (WACCM-X), a leading general circulation model. We find that although most of the seasonal cycle in the winds is captured well, WACCM-X exhibits biases in the winds at upper heights. In wintertime, the zonal winds are westwards whereas in observations they are eastward. In summertime WACCM-X model meridional winds at 90–100 km are southwards but observations northwards. The observed and modeled winds also display significant interannual variability. We characterize the trends of the winds and the correlation with various drivers (the 11-year solar cycle, El Niño Southern Oscillation, the Quasi-Biennial Oscillation and the Southern Annular Mode), using a multi-linear regression method. The study uses a uniquely long data set of Antarctic MLT winds to test and further develop general circulation models and quantifies the relationship between these winds and drivers such as the solar cycle.

## 1. Introduction

The winds in the mesosphere and lower thermosphere (MLT) are strongly influenced by gravity wave driving. Gravity waves generated at lower heights propagate upwards into the MLT, growing in amplitude before breaking and depositing their momentum after they break and thus driving the winds (Fritts & Alexander, 2003; Smith, 2012).

© 2024. The Authors.

This is an open access article under the terms of the [Creative Commons Attribution License](https://creativecommons.org/licenses/by/4.0/), which permits use, distribution and reproduction in any medium, provided the original work is properly cited.

**Funding acquisition:** Nicholas J. Mitchell, Tracy Moffat-Griffin  
**Investigation:** Phoebe E. Noble  
**Methodology:** Phoebe E. Noble, Neil P. Hindley, Corwin J. Wright, Chihoko Cullens, Nicholas J. Mitchell, Tracy Moffat-Griffin  
**Project administration:** Corwin J. Wright, Nicholas J. Mitchell, Tracy Moffat-Griffin  
**Resources:** Chihoko Cullens  
**Software:** Phoebe E. Noble, Neil P. Hindley  
**Supervision:** Neil P. Hindley, Corwin J. Wright, Nicholas J. Mitchell, Tracy Moffat-Griffin  
**Validation:** Phoebe E. Noble  
**Visualization:** Phoebe E. Noble  
**Writing – original draft:** Phoebe E. Noble, Corwin J. Wright, Chihoko Cullens, Nicholas Pedatella, Nicholas J. Mitchell, Tracy Moffat-Griffin  
**Writing – review & editing:** Phoebe E. Noble, Neil P. Hindley, Corwin J. Wright, Chihoko Cullens, Scott England, Nicholas Pedatella, Nicholas J. Mitchell, Tracy Moffat-Griffin

This process poses unique problems for models of the planetary scale circulation because the details of gravity wave driving remain poorly understood, largely due to limited measurements of the wind in the MLT region. This limitation is particularly so in Antarctica where instrument deployment is logistically difficult. Nevertheless, the Antarctic Peninsula and nearby Southern Andes mountain ranges are one of the largest orographic gravity wave source regions (Hoffmann et al., 2013). This makes observations here vital in understanding the gravity wave driven dynamics and constraining models in this region.

The general circulation of the MLT is known to display a clear seasonal cycle. The meridional wind of the MLT is dominated by the global pole-to-pole circulation of the gravity wave driven upper branch of the Brewer-Dobson circulation (also known as the residual circulation). Further, there is good evidence that there is significant interannual variability in the winds (Baumgaertner et al., 2005; Dowdy et al., 2007; Sandford et al., 2010) and a number of studies have attempted to quantify and explain the physical causes of this variability. However, such studies are often limited by the relatively small number of reliable observational data sets available of long enough duration. Despite this difficulty, some observational studies have explored the possible influence of the solar cycle on the winds in the MLT region (e.g., Bremer et al., 1997; Cai et al., 2021; Greisiger et al., 1987; Jacobi et al., 1997; Jaen et al., 2023; Middleton et al., 2002; Wilhelm et al., 2019). However, as noted by Cai et al. (2021), results from such studies vary by location and time period used. Karlsson and Kuilman (2018) investigated the influence of the solar cycle on the middle atmosphere residual circulation near the solstices in CMAM30 (the Canadian Middle Atmosphere Model for 1979–2009) and proposed a mechanism wherein at high solar activity, the residual circulation was strengthened due to the influences of enhanced heating affecting temperature gradients and the filtering of gravity waves. This is a potential mechanism for solar modulation of MLT winds. Similarly, other atmospheric phenomena have been proposed to affect the winds in the MLT. Observational evidence of an influence from the El Niño Southern Oscillation (ENSO) has been reported by Li et al. (2016), Llamedo et al. (2009), Sundararajan (2020) and Kishore et al. (2014) for the stratosphere/mesosphere at various different locations. Some studies (Ford et al., 2009; Kishore et al., 2014) report an influence from the Quasi-Biennial Oscillation (QBO) on MLT winds. However, Baumgaertner et al. (2005) found no such influence from the solar cycle, ENSO or the QBO on MF radar observed Antarctic winds. In addition, the influence of the Southern Annular Mode (SAM) on MLT winds has not been widely explored aside from briefly in Merzlyakov et al. (2009) where no link was found with winter winds.

Modeling studies have also investigated the interannual variability of the MLT and attempted to identify the causal drivers of such variability. In particular, Cullens et al. (2016) inspires the basis for this study wherein they used Whole Atmosphere Community Climate Model (WACCM) (version 4) to explore the influence of the 11-year solar cycle on atmospheric winds globally. They found that in the southern hemisphere there are statistically significant changes in gravity wave drag and associated winds that are likely due to the solar cycle. Gan et al. (2017) and Ramesh et al. (2020) used a linear regression method to investigate the interannual variability of winds and temperatures in the global climate models eCMAM and WACCM, respectively. This method was used to attribute changes in the winds and temperatures to different drivers. Both Gan et al. (2017) and Ramesh et al. (2020) found a positive temperature response to higher levels of solar irradiance for all latitudes in the mid stratosphere and upwards, with the strength of the correlation increasing with height. In addition to this temperature response, both Gan et al. (2017) and Ramesh et al. (2020) found changes in the wind correlating with the solar cycle, although these were more varied than the temperature responses and were latitude and height dependent.

In this work we present a long-term study (2005–2021) of the interannual variability of Antarctic winds from a meteor radar equipped with height resolving capabilities and compare these observations to the predictions of WACCM-eXtended (WACCM-X) for the same location. WACCM-X is the eXtended version of the Whole Atmosphere Community Climate Model, a general circulation model based on Community Earth System Model (CESM), more details can be found in Section 2.2.

Long-term Antarctic MLT winds have been explored in the past by meteor radars without height resolving ability (e.g., Merzlyakov et al., 2009; Portnyagin et al., 1992). Whilst some of these studies span a longer time period than that considered here, the MLT winds have strong variation with height which could not be addressed by these meteor radars. Other long-term work has used observations from MF radars (e.g., Baumgaertner et al., 2005; Dowdy et al., 2007; Iimura et al., 2011; Merzlyakov et al., 2009; Portnyagin et al., 1992), however, MF radars

have known and significant biases in winds measured at heights above  $\sim 90$  km (Jacobi et al., 2009; Manson et al., 2004; Wilhelm et al., 2017). Meteor radars are generally free from these biases.

Here we use data recorded from 2005 to 2021 by the Rothera meteor radar and build upon work done earlier by Sandford et al. (2010) who reported first results from this radar and compared them to winds measured at Esrange ( $68^{\circ}\text{N}$ ,  $21^{\circ}\text{E}$ ), in the Arctic. The radar at Rothera has an interferometer to determine meteor heights and has been running since 2005. This unique combination yields a data set ideally suited to investigate seasonal and interannual variability. Our goal is to determine the seasonal and interannual variability found in this long radar data set and compare the winds to the WACCM-X model. We use a linear regression method to explore the relationship between both observed and modeled MLT winds with four particular potential phenomena, namely, (a) the 11-year solar cycle, (b) the ENSO, (c) the QBO and (d) the SAM.

In Section 2 we present the meteor radar data, WACCM-X data and climate indices for the linear regression. Section 3 describes the linear regression method used to explore the interannual variability. The results are split over two sections with Section 4 presenting and comparing the wind climatologies from both the radar observations and WACCM-X model. Section 5 presents the results from the linear regression. The discussion can be found in Section 6 and conclusions in Section 7.

## 2. Data

### 2.1. Meteor Radar

In this study we use wind data from the SKiYMet all sky radar at Rothera on the Antarctic Peninsula ( $67^{\circ}\text{S}$ ,  $68^{\circ}\text{W}$ ). The radar was installed in February 2005. It uses a peak power of 6 kW and operates with a radio frequency of 32.5 MHz. The antennas were replaced in February 2019 due to hardware degradation and the PRF was changed from 2144 Hz to 625 Hz at the same time in order to bring it in line with current operating radars, this change does not have an effect on the determination of the mean wind. Further details on the configuration of this particular radar can be found in Sandford et al. (2010) and a complete description of meteor radar processing methods in Hocking et al. (2001). Here we derive hourly zonal and meridional wind values from meteor echoes for heights of 80–100 km. A collection of meteor echoes is needed to determine the horizontal wind. We use a Gaussian weighting in height and time with a full width half maxima of 2 hr in time and 3 km in height. This Gaussian weighting is then stepped by 1 hr in time and 1 km in height. For a complete description of this method see Hindley et al. (2022).

The meteor radar data is presented in Figure 1. Panel (a) shows the location of the meteor radar on the Antarctic Peninsula indicated by a red dot. The surrounding blue dots show the spacial distribution of meteor echoes detected over one day (1 July 2005), this serves to demonstrate that the distribution of meteor radar echoes around the radar are not biased in any direction. Panels (b) and (c) present the distribution of meteors over 1 month, with panel (b) showing their distribution in height, indicating that although the meteor count peaks at 90 km, there are sufficient meteors to derive wind information between 80 and 100 km. In panel (c), we show the diurnal cycle of meteor counts, with again sufficient meteor counts to determine wind information even at the minimum count.

There are some notable periods of poor data quality. Radio interference reduced data quality in the interval December 2009 to January 2010. December 2010 also experienced interference from an unknown source (possibly summertime base activities at the British Antarctic Survey base at Rothera). The largest period of poor data quality takes place in the years preceding the replacement of the antennas due to degradation of the hardware because of repetitive freeze-thaw cycling. For this reason, we exclude the three years, 2016–2018 from the meteor radar data. These periods are identified either by abnormal meteor count or an unusual distribution of the zenith angle of the meteors (caused by poor determination of the zenith angle, indicative of hardware failure). The zenith angle distribution through time is presented in the Supporting Information S1.

### 2.2. WACCM-X

The WACCM is a General Circulation Model (GCM) which simulates the atmosphere from the surface to the lower thermosphere ( $\sim 140$  km). WACCM-X, reaches to the upper thermosphere and includes additional thermodynamic processes and ionospheric electrodynamics (Liu et al., 2018). The numerical framework for WACCM-X is based on the CESM. WACCM-X includes chemical, dynamical and physical processes to model the lower, middle, and upper atmospheres (Marsh et al., 2013; Neale et al., 2013). Gravity waves are modeled

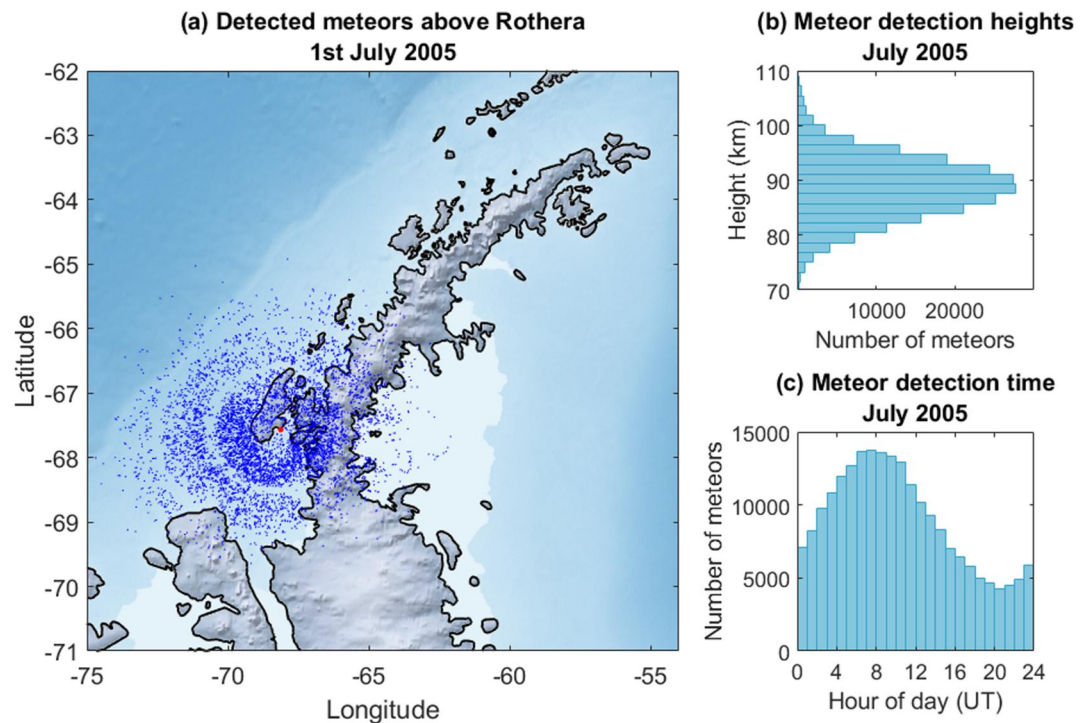


**Figure 1.** (a) The spatial distribution of meteors recorded over Rothera on one day, 1 July 2005. Individual meteors are shown in blue and the radar location in red (b) The height distribution of meteors recorded over 1 month, July 2005 (c) A histogram of hourly meteor counts recorded over 1 month, July 2005.

using a parametrization based on Lindzen (1981) and Richter et al. (2010). The model resolution is  $2.5^\circ$  latitude by  $1.9^\circ$  longitude. The vertical resolution is one-quarter scale height above 1 hPa.

We use data for 2005–2021 (inclusive) from the specified dynamics version of WACCM-X version 2.1 extended runs. This nudges to Modern-Era Retrospective analysis for Research and Applications, Version 2 (MERRA-2) data from the surface up to heights of  $\sim 50$  km (Noble, 2023). The details and validation of WACCM-X 2.0 can be found in Liu et al. (2018). For direct comparability with the meteor radar data we extract data from WACCM-X using the 3-hourly output as follows. Firstly, the meteor radar measures winds over a horizontal collecting region of several hundred km diameter (as shown in Figure 1a). To enable comparison with the model, we average the WACCM-X winds over all grid points that lie within this region. Secondly, as a height coordinate, we take the geopotential height from WACCM-X, convert to geometric height and interpolate onto the meteor radar height grid. We again take monthly mean and average year wind values in the zonal and meridional components for comparison with the radar observations. For complete fairness in our linear regression, we remove the months from WACCM-X where the radar data is not useable.

### 2.3. Climate Indices

To explore potential drivers of interannual variability in the MLT winds, we regress our monthly mean winds against time and a number of climate indices, specifically the 11 years solar cycle, ENSO, the QBO and the Southern Annular Mode (SAM, also known as the Antarctic Oscillation). These phenomena are described below, summarized in Table 1 and presented in Figure 2. F10.7, ENSO, QBO10 and QBO30 are used in the regression with no pre-processing, however, the seasonal cycle is removed from the SAM index (mean year subtracted from each year), because the seasonal cycle dominates the SAM. In Table 1 we also present  $\alpha$ , this is the scaling used to present the regression results. For solar, we scale by 100 sfu, for comparability with other studies. For the other indices, ENSO, QBO10, QBO30 and SAM, we scale by the interdecile range which is defined as the 90th percentile minus the 10th percentile. This scaling choice allows the regression results interpreted as the change in the winds given a change in the index from its minimum to maximum value (whilst allowing for outliers).

**Table 1**  
Summary of Climatological Indices Used in This Study

Climatological index	Scaling ( $\alpha$ )	Description	Data source
Time	10 years	Number of months since January 2005	N/A
Solar	100 sfu	Observed solar irradiance at the 10.7 cm wavelength	National Research Council of Canada
ENSO	2.7 °C	Nino 3.4 index	Trenberth (2022)
QBO10	45 ms <sup>-1</sup>	Zonal-mean zonal-winds between 5°N and 5°S at 10 hPa height	ERA5
QBO30	42 ms <sup>-1</sup>	Zonal-mean zonal-winds between 5°N and 5°S at 30 hPa height	ERA5
SAM	3.9 hPa	Pressure difference between six observational stations around 65°S and six stations around 40°S. SAM anomaly used (seasonal cycle removed)	Marshall (2018)

Note. The scaling for El Niño Southern Oscillation, QBO10, QBO30 and Southern Annular Mode is the interdecile range defined as the 90th percentile minus the 10<sup>th</sup> percentile and is a measure of the spread of the index. For solar, we use the standard 100 sfu for Comparability with existing studies and for time we use 10 years.

These indices (except for SAM) are chosen as previous work has found some link between the phenomena and the MLT dynamics. Studies for the 11-year solar cycle include Greisiger et al. (1987); Bremer et al. (1997); Jacobi et al. (1997); Middleton et al. (2002); Cullens et al. (2016); Wilhelm et al. (2017); Ramesh et al. (2020); French et al. (2020a); Cai et al. (2021). For the El Niño Southern Oscillation, Llamedo et al. (2009); Li et al. (2016); Ramesh et al. (2020). Finally, Ford et al. (2009) and Ramesh et al. (2020) found links between the MLT and QBO. To represent the QBO we use two indices, QBO10 and QBO30, a measure of the equatorial winds at two different pressure heights (10 and 30 hPa). These two heights are chosen as these two indices are often used together in atmospheric regression studies (Bojkov & Fioletov, 1995; Nair et al., 2013; Ramesh et al., 2020) to capture possible influences of the QBO, additionally the two time series are almost orthogonal (Chiodo et al., 2014). The SAM is the dominant mode of atmospheric variability in the Southern Hemisphere (Marshall, 2003) and beyond

### Linear regression indices

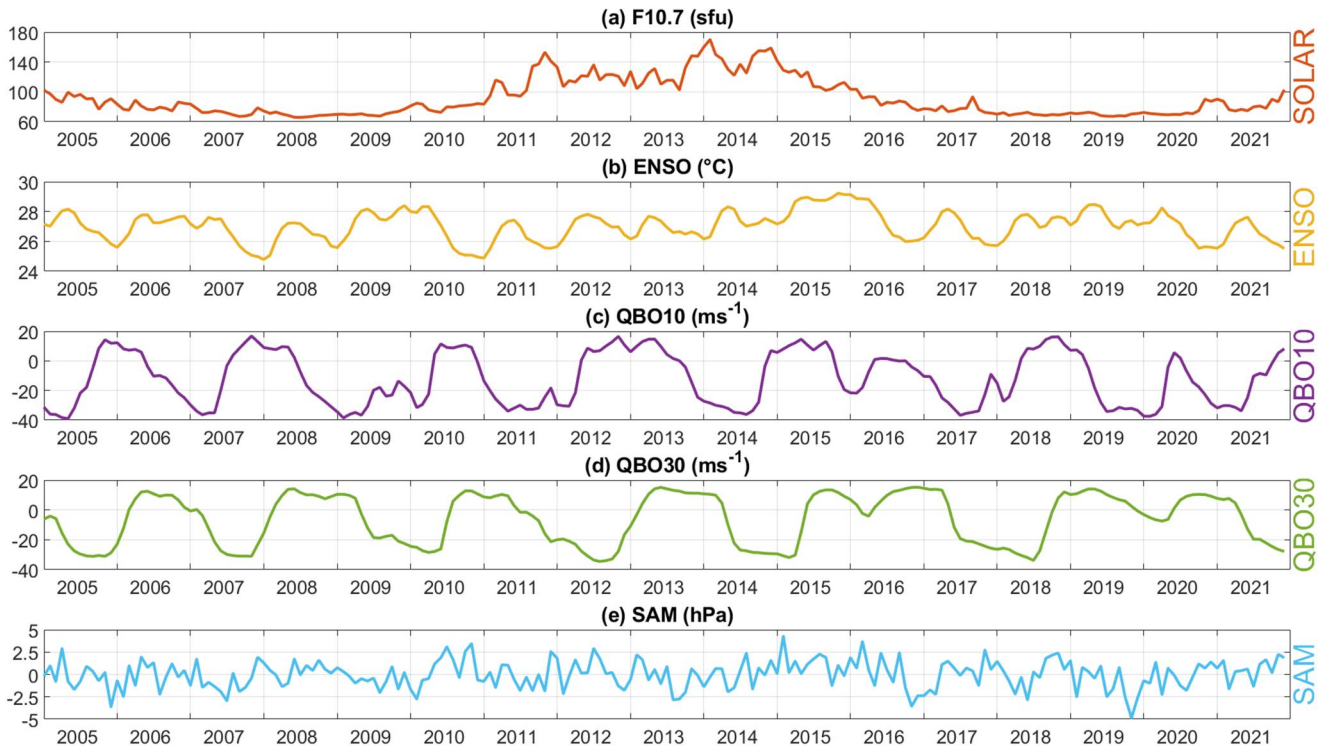


**Figure 2.** Time series of the climatological indices used in our linear regression analysis from 2005 to 2021. The source of each index is given in Table 1.

the Antarctic, the SAM has been found to have influences on the climate in Australia, South Africa and other Southern Hemisphere countries (Gillett et al., 2006). We speculate however, that as a Southern Hemispheric oscillation, the SAM is often excluded from linear regression studies of global models where regional oscillations are not considered (Gan et al., 2017; Ramesh et al., 2020).

The list of indices used in this regression study are by no means the only possible drivers of variability of the winds in the Antarctic MLT. Ozone, CO<sub>2</sub> concentrations, the timing of the breakdown of the polar vortex or other atmospheric oscillations could also contribute to the variability. For example, French et al. (2020b) found evidence of a quasi-quadrennial oscillation in temperature in the polar mesosphere and highlighted the inter connectivity of our entire atmosphere–ocean system. Throughout this study we are aware of these potential drivers but are restricted by the number of independent variable we can include to avoid over fitting our linear regression model and therefore have chosen those five indices we regard as most important. CO<sub>2</sub> is specifically omitted due to its strong correlation with time.

### 3. Method

#### 3.1. Linear Regression Analysis

To carry out our linear regression we use monthly mean winds in the zonal and meridional components from the radar observations and WACCM-X predictions. To start, we apply a similar method to (Gan et al., 2017; Ramesh et al., 2020) by considering the wind anomaly for each month. This wind anomaly is defined as the deviation of each month from the climatological mean. This removes the seasonal cycle revealing only interannual variability.

We next separate our data and build a multilinear regression model for each month using a 3 month window centered on the month of interest. The linear regression analysis is carried out on each height level for the meridional and zonal winds independently. We propose and apply the following linear regression model and use the Ordinary Least Squares (OLS) method to estimate the  $\beta$  coefficients.

$$\Psi = \beta_0 + \beta_1 \times \text{TIME} + \beta_2 \times \text{SOLAR} + \beta_3 \times \text{ENSO} + \beta_4 \times \text{QBO10} + \beta_5 \times \text{QBO30} + \beta_6 \times \text{SAM} + \epsilon, \quad (1)$$

where  $\Psi$  is the wind anomaly (for radar or WACCM-X winds, zonal or meridional wind component),  $\epsilon$  is the residual,  $\beta_0$  is the regression constant and  $\beta_1, \beta_2, \dots, \beta_6$  are the regression coefficients which are determined by linear regression. Solar, ENSO, QBO10, QBO30 and SAM are the climate indices described in Section 2.3 and are functions of time. Statistical significance of each regression coefficient is determined using Student's T-test.

Linear regression is a powerful tool for identifying relationships between variables and it allows us to decompose the wind anomaly into component parts that we may attribute to various drivers. However, the application requires some care in the interpretation of the results. Firstly, linear regression is by definition, linear, but the atmosphere is not in general a linear system. As such, any results are potentially a simplification of the interactions that are occurring. Secondly, we note that the results presented in this study do not necessarily mean causation, and a correlation between the winds and the indices could be a coincidence and not a causal link. Despite these points, this analysis allows us to investigate the linear influences of atmospheric and solar oscillations on the winds in the Antarctic MLT and thus gain useful insights into potential drivers of variability.

##### 3.1.1. Multicollinearity

To ensure the regression analysis is valid, we must check that there is no correlation between our independent variables (time, F10.7, ENSO, QBO10, QBO30 and SAM). The presence of a correlation is called multicollinearity and would lead to biased coefficients and standard errors in the regression. To check for this, we consider the variance inflation factors (VIFs) between the independent variables (Montgomery, 2012; Nair et al., 2013). Possible values of the VIF range from 1 to infinity. VIF values and their meanings can be found in more details in Gareth et al. (2013); Kutner et al. (2005) and We summarize them here: A VIF near one indicates there is no multicollinearity while VIFs between 1 and 5 suggest some multicollinearity but not enough to require adaption to the model. Values over 5 are cause for concern and values over 10 are a major problem and the model will require adaptation. Our VIFs range from 1.02 to 1.28 and we conclude that these independent variables do not suffer from significant multicollinearity and we can safely proceed. Further details on the VIF calculation can be found in the Supporting Information S1.

### 3.1.2. Auto-Correlation

Another assumption of linear regression is that the residuals (the difference between the regression model's predicted value and the actual value) are free from auto-correlation, that is, that the residuals from the regression analysis are not correlated with each other. Auto-correlation indicates that important information is missing from the model and the standard errors cannot be relied upon.

To test for auto-correlation, we use the Durbin Watson (DW) test, we summarize this method in the Supporting Information S1 and further details can be found in Webster (2012). This tests for serial correlations and is based on the correlation between model residuals. The residuals are the difference between the linear regression model predicted values and the actual values. The output of the DW test is a number in the range (0, 4) (where square brackets indicate the closed interval). A result of 2 means that there is no auto-correlation present, results closer to 0 mean positive auto-correlation and toward 4 means negative auto-correlation. Generally, values between 1.5 and 2.5 are acceptable (Sofroniou & Hutcheson, 1999), whilst results below 1 and above 3 can be cause for concern (Field, 2013). We apply the DW test to each regression performed in the study that is, each 3 month model, each wind direction and for the meteor radar and WACCM-X data separately. For the regressions run on radar data 88% lie in the interval (1.5, 2.5) and 98% in (1, 3). For WACCM-X regression, 84% lie within (1.5, 2.5) and greater than 99% lie within (1, 3). Any deviation from a DW result of two indicates that some auto-correlation is present, however, almost all of our DW statistics lie in the acceptable (1, 3) region. So whilst there will be some uncertainty over the standard errors for a small minority (<1%) of models, the large majority of models do not suffer from this problem.

## 4. Results: The Winds in Radar Observations and WACCM-X

### 4.1. Zonal Winds

The monthly mean zonal winds are presented in Figure 3. The first row shows the average year, with panel (a) the radar observations and (b) the WACCM-X predictions and (c) their difference. In the observations, the zonal wind is characterized by the summertime wind reversal where the wind below heights of about 90 km reverses from eastwards to become westwards throughout the Antarctic summer (October–March), maximizing at speeds of  $\sim -35 \text{ ms}^{-1}$  at the lowest heights observed. The eastward winds maximize in February, above the zero-wind line at heights of 95–100 km. The summertime wind reversal in WACCM-X has a similar temporal pattern, with the reversal to summertime westward winds beginning in October. However, the westwards winds in the WACCM-X reversal are stronger, maximizing at  $-45 \text{ ms}^{-1}$  at heights near 80 km. However, the most notable difference between the observations and the model occurs in April–October at heights of 85–100 km where WACCM-X predicts westward winds of up to  $10 \text{ ms}^{-1}$ , but the radar observations reveal eastward winds of magnitude  $10\text{--}15 \text{ ms}^{-1}$ . From panel (c), we can see that throughout wintertime (April–September), the winds are more westwards in WACCM-X at all heights and up to  $20 \text{ ms}^{-1}$  more westwards at upper heights around August. In summary, the two main differences in the zonal wind between the observations and the model are as follows.

- For wintertime winds (April–September) at heights of 85–100 km, the radar observations show eastward winds of magnitude  $10\text{--}15 \text{ ms}^{-1}$ , whilst WACCM-X has westward  $5\text{--}10 \text{ ms}^{-1}$  winds.
- The maximum wind speeds in the summer wind reversal (October–March) are weaker in radar observations than in WACCM-X.

The full timeseries of monthly mean winds for the radar and WACCM-X, respectively, are shown in panels (d) and (e). We draw attention to the zonal wind wintertime bias (April–September) that appears every single year as a persistent feature, that is, observed wintertime winds at heights of 85–100 km are eastwards but WACCM-X predicted winds are westwards.

### 4.2. Meridional Winds

In Figure 4 we show the meridional component of the wind, with panels (a) and (b) presenting the average year for the radar and WACCM-X respectively. In the radar wind observations and WACCM-X we see the MLT Brewer–Dobson circulation at heights of 80–90 km where in winter the wind becomes southwards. Throughout summer, the winds are northwards, flowing away from the pole.

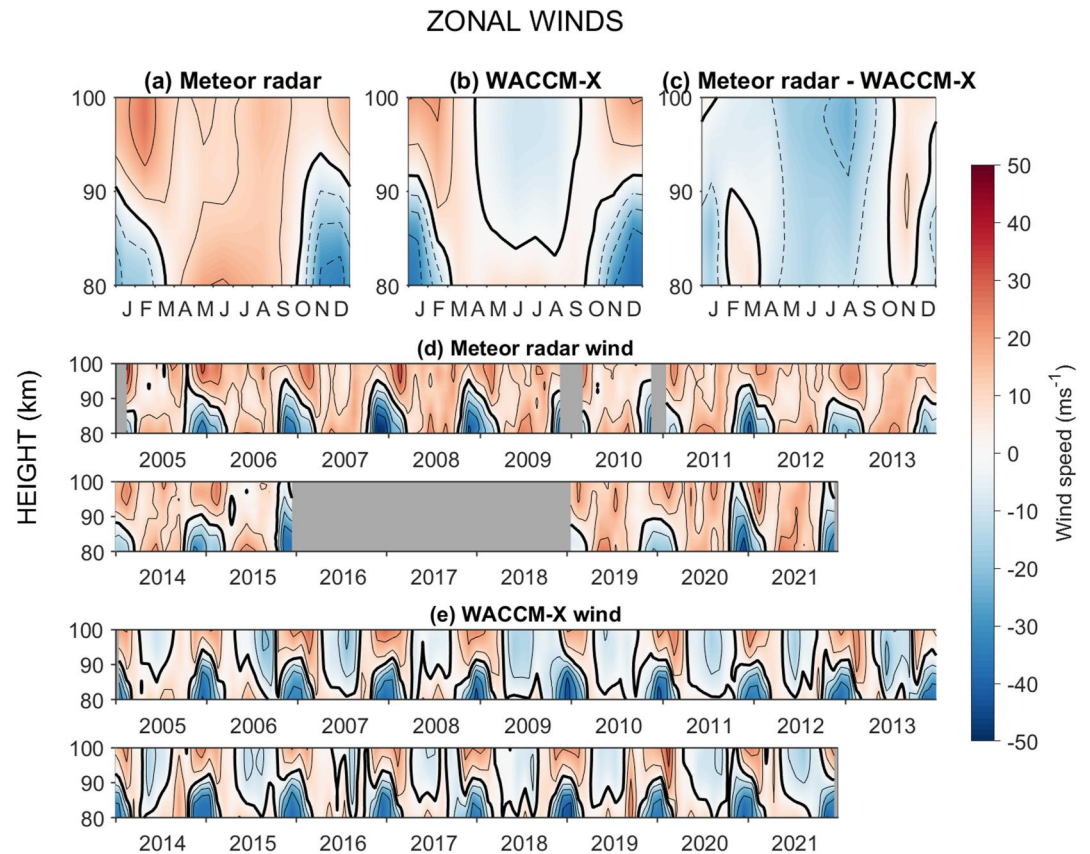


**Figure 3.** Monthly mean zonal winds as a function of height and time. (a) Radar observations average year, (b) the eXtended version of the Whole Atmosphere Community Climate Model (WACCM-X) predictions average year, (c) Meteor radar observations average year minus WACCM-X average year. (d) Monthly mean winds from the radar observations for the interval 2005–2021, (e) Corresponding monthly mean winds from WACCM-X for the interval 2005–2021. Solid black line indicates the zero-wind contour line and the contour interval is  $10 \text{ ms}^{-1}$ .

Similarly to the zonal component, we also note a persistent bias when comparing the observations to the model. However, this occurs in the summer (unlike the zonal wind bias which occurs in wintertime). In particular, in summer, at heights of 90–100 km WACCM-X predicts southwards flow, but the radar results reveal northward winds throughout the whole year at this height. In the difference plot, panel (c), we find that the largest difference between model and observations is in October–December toward the upper heights where the meteor radar reveals winds that are over  $15 \text{ ms}^{-1}$  more northwards. In panels (d) and (e) we can see that this difference is present in all years.

To summarize, the main difference between the radar observations and WACCM-X predictions in the meridional component is.

- During Antarctic summer at heights above 90 km the wind observed by the radar is northwards but in the WACCM-X prediction it is southwards.
- The largest magnitude difference occurs in October–December at upper heights where the winds are over  $15 \text{ ms}^{-1}$  more northwards in radar observations than WACCM-X.

### 4.3. Interannual Variability

As can be seen in Figures 3 and 4, panels (d) and (e), there is significant interannual variability evident in both wind components and in both the radar results and the WACCM-X predictions. In the zonal component of the radar observations, the shape and magnitude of the summertime wind reversal and the eastward winds above it change every year for example, the wind reversal at the end of 2007 is far stronger than that of 2019.



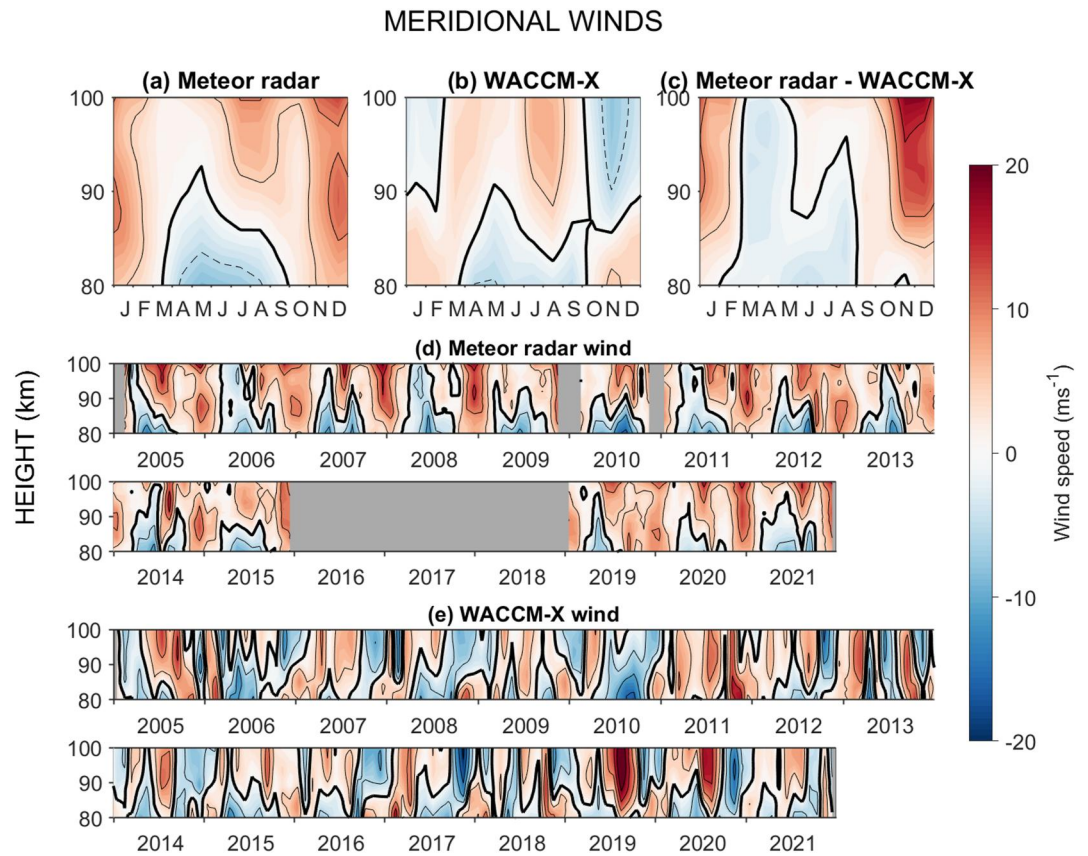


**Figure 4.** Monthly mean meridional winds as a function of height and time. (a) Radar observations average year, (b) the eXtended version of the Whole Atmosphere Community Climate Model (WACCM-X) predictions average year, (c) Meteor radar observations average year minus WACCM-X average year. (d) Monthly mean winds from the radar observations for the interval 2005–2021, (e) Corresponding monthly mean winds from WACCM-X for the interval 2005–2021. Solid black line indicates the zero-wind contour line and the contour interval is  $5 \text{ ms}^{-1}$ .

Figure 5 shows the interdecile range of each month at heights of 85 and 95 km, for the radar and WACCM-X monthly mean winds, and for zonal and meridional components. The interdecile range is the 90th percentile minus the 10th percentile, which gives a measure of the variation in the monthly mean wind speeds across the years considered. In (a), it can be seen that the interdecile range of the meteor radar observed zonal wind maximizes in the summer, when the zonal wind reversal occurs, due to the variability in the strength and timing of this reversal. Whereas for WACCM-X the peak is earlier in the year. For both heights, there is more variability in

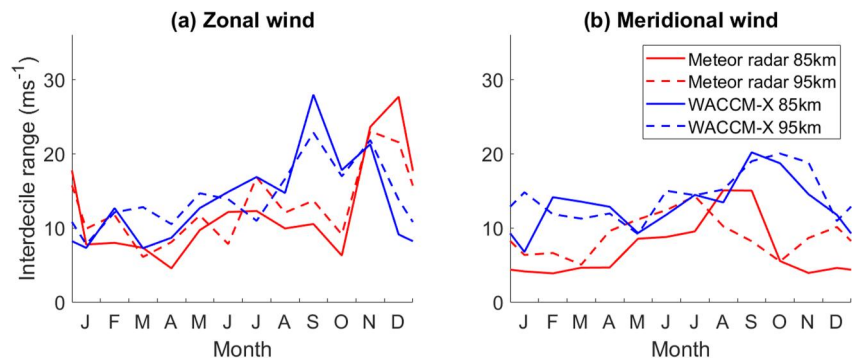


**Figure 5.** A measure of the interannual variability of the monthly mean winds. The interdecile range (90th percentile minus 10th percentile) of zonal and meridional winds for each month. Figures show radar data (red) and the eXtended version of the Whole Atmosphere Community Climate Model data (blue) at two heights, 85 km (solid line) and 95 km (dashed line).

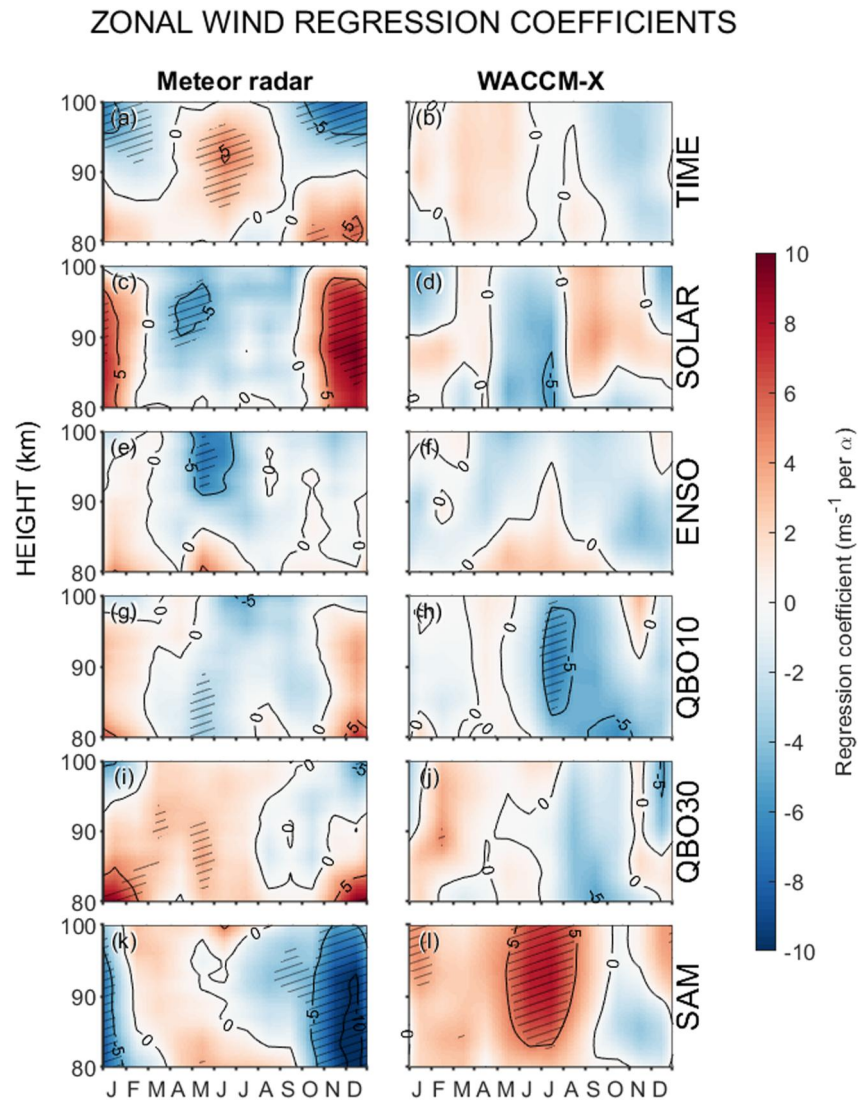


**Figure 6.** Regression coefficient from the linear regression analysis for the zonal winds. Left column is results from radar observed winds, right column is from the eXtended version of the Whole Atmosphere Community Climate Model predicted winds. First row is the coefficient results from the time term in the linear regression, second row solar term, third row El Niño Southern Oscillation term, fourth row QBO10 term, fifth row QBO30, and bottom row Southern Annular Mode term. Units are  $\text{ms}^{-1}$  per  $\alpha$ , where  $\alpha$  is defined in Table 1. Hatching indicates regions statistically significant at the 95% level. Each regression coefficient and statistical significance level is determined using data from a 3-month window, stepped by 1 month, and displayed at the location of the center month.

WACCM-X than the radar observations for the first 10 months of the year. In panel (b), the interdecile range of the meridional winds observed by radar peaks in the winter, indicating variations in the strength of the MLT Brewer-Dobson circulation. Similarly to the zonal direction, in the meridional direction, the interdecile range in the WACCM-X is higher than the meteor radar observations.

## 5. Results: Linear Regression Analysis

### 5.1. Trends With Time

In Figure 6 we present the results from the linear regression analysis for the zonal wind. The first row shows the results from the time term in the linear regression, that is,  $\beta_1$  from Equation 1. Each regression coefficient value and statistical significance level is calculated and presented on the figure at the location of the center month of the 3 month windows. Hatching indicates where the relationship is statistically significant at the 95% level, using the

Student's t-test. Throughout the results and discussion we refer to results that are significant at this 95% level as statistically significant. For this independent variable we assign  $\alpha = 120$  months, this gives the change in the wind in  $\text{ms}^{-1}$  per decade. The full description of the  $\alpha$  values chosen for each term is given in Table 1.

The most striking and significant trends are seen in Figure 6 panel (a), for the zonal wind recorded by the meteor radar. Here we find a significant weakening of the westwards summertime wind at lower heights (October–December at heights of 80–90 km), with the regression results suggesting that the winds are becoming more eastwards at a rate of up to  $5 \text{ ms}^{-1}$  per decade. At the same time, the eastwards winds above (95–100 km) are weakening also, at rates of up to  $7 \text{ ms}^{-1}$  per decade, with this change extending throughout the summer into January and February. The wintertime (May–July) eastwards winds at 85–95 km are strengthening with time. For the equivalent zonal wind results from WACCM-X there are absolutely no significant trends in time.

The equivalent for meridional wind is shown in Figure 7. The meteor radar observations (panel a) show no significant trends in time, whereas the model predictions (panel b) show an northwards trend in July and August at heights of 90–100 km.

## 5.2. The 11 Years Solar Cycle

The results from the solar term are presented in panels (c) and (d) in Figures 6 and 7. The colored contours show the difference we see in wind speeds for a 100 sfu increase in F10.7, that is,  $\alpha = 100\text{sfu}$ . Statistically significant differences at the 95% level are hatched.

In the regression results from the radar zonal-winds for the solar term (Figure 6c), the biggest region of significance is in November and December at heights of 80–98 km, where we see a response of up to  $8 \text{ ms}^{-1}$  per 100 sfu eastwards. This can be interpreted to mean that the linear regression fit to the winds suggests that were F10.7 to increase by 100 sfu the winds would be  $8 \text{ ms}^{-1}$  more eastwards. This result suggests that during a solar maximum, the summertime westward winds at the lower heights are weaker and the strength of the eastwards winds above increased. Another, significant time of year with a negative response is found in April–May at heights of 90–97 km of magnitude up to  $5 \text{ ms}^{-1}$  per 100 sfu. However, again like the results from the time term, there is no significant correlations between F10.7 and the WACCM-X zonal winds at the 95% significance level.

Figures 7a and 7b show the results for the meridional wind. In the radar observed winds we see a small statistically significant negative correlation at heights of 97–100 km throughout the summer. In the results from WACCM-X, again the vast majority of correlations are not significant.

## 5.3. The El Niño Southern Oscillation

We present the results from the ENSO coefficient in (Figures 6e, 6f, 7e, and 7f). This term is scaled by the interdecile range of the ENSO index, to give a representation of the change in winds between a typical El Niño ( $25.8^\circ\text{C}$ ) and La Niña event ( $28.5^\circ\text{C}$ ).

At heights of 90–100 km, we see large values of this coefficient in both zonal and meridional (although only significant in the zonal direction) components during May–June. This implies that there are stronger north westwards winds when the ENSO index is large that is, an El Niño event. In WACCM-X there is almost no significant correlation between the ENSO index and the winds.

## 5.4. The Quasi-Biennial Oscillation

There is no agreement between the coefficient results from the radar and WACCM-X in either zonal (Figures 6g and 6h) or meridional components (Figures 7g and 7h) for the QBO10 index. In the zonal direction for the radar observed winds (Figure 6g), when the QBO10 index is larger (i.e., a westerly phase), the results suggests a generally eastwards change in the winds in the summer and a westwards wind influence in the winter, however, the significant regions are almost negligible. In WACCM-X zonal winds (Figure 6h) we see a large significant negative wind correlation between the zonal winds and the QBO10 index in July–August. In the meridional direction (Figures 7g and 7h), the WACCM-X results show that the winds are significantly more westwards during May–July at heights of 80–90 km and at all heights in July, this suggests that the summertime westwards winds in WACCM descend lower during the westerly phase of the QBO.

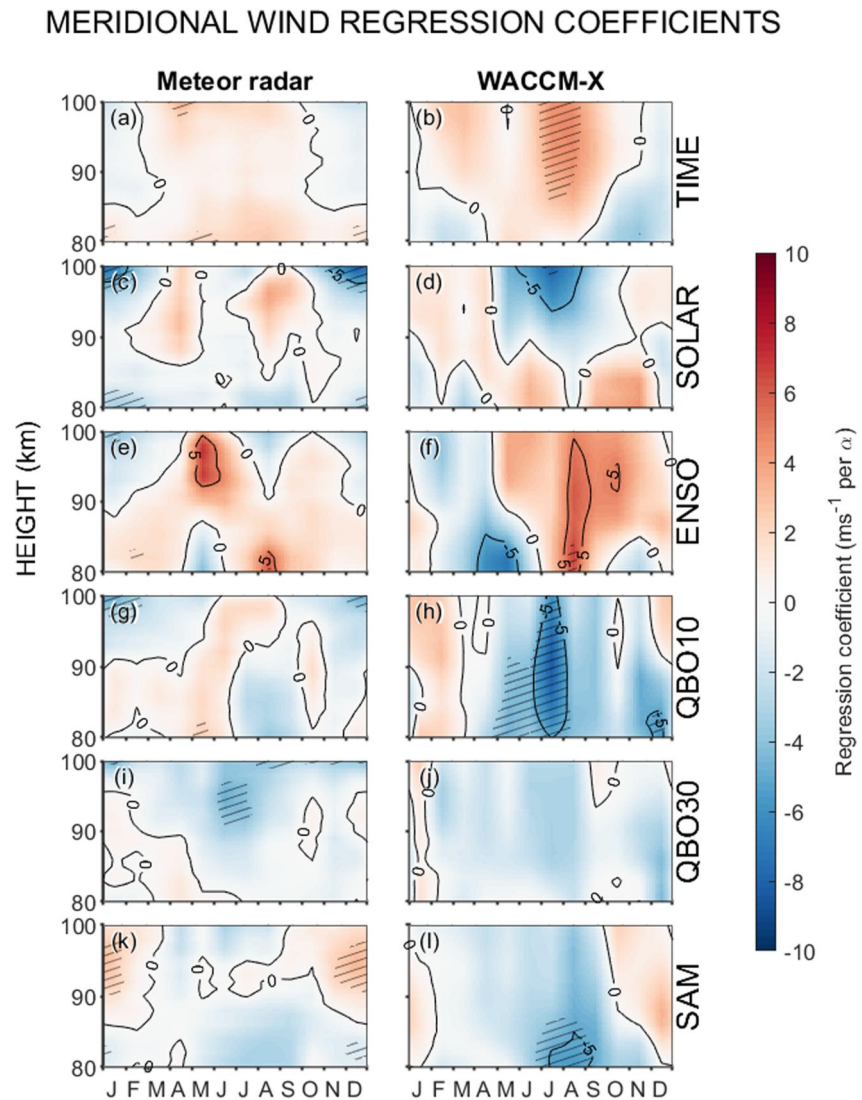


**Figure 7.** Regression coefficient from the linear regression analysis for the meridional winds. Left column is results from radar observed winds, right column is from the eXtended version of the Whole Atmosphere Community Climate Model predicted winds. First row is the coefficient results from the time term in the linear regression, second row solar term, third row El Niño Southern Oscillation term, fourth row QBO10 term, fifth row QBO30, and bottom row Southern Annular Mode term. Units are  $\text{ms}^{-1}$  per  $\alpha$ , where  $\alpha$  is defined in Table 1. Hatching indicates regions statistically significant at the 95% level. Each regression coefficient and statistical significance level is determined using data from a 3-month window, stepped by 1 month, and displayed at the location of the center month.

In the coefficient results for QBO30 there are some non-significant similarities between the radar wind results and WACCM-X results. In the zonal component (Figures 6i and 6j), we see results suggesting that the wind is generally more eastwards during the first half of the year, and more westwards in the later half (August–December). However, the regions that are significant again do not coincide. In the meridional component (Figures 7i and 7j), an increase in the QBO30 index suggests winds are more southwards. The radar meridional results also see a stronger, significant, southwards wind response during June–July around 90–97 km.

### 5.5. The Southern Annular Mode

The bottom row in Figures 6 and 7 shows the regression coefficient results from our final index, the Southern Annular Mode (SAM). The SAM index exhibits its largest correlation with the winds in the zonal component (Figures 6k and 6l) whilst the meridional results see fewer significant areas (Figures 7k and 7l).

In the zonal winds, we find conflicting correlations between the observed winds and WACCM-X prediction. In the observations, we see the strongest response in November–January, where the results show that for increase of  $\alpha = 3.9$  hPa in the SAM index, the zonal winds are  $10 \text{ ms}^{-1}$  more westwards. This contributes to a stronger and higher-reaching summertime reversal. However, the linear regression results from WACCM-X predict no correlation in November–January, but show a large significant eastwards correlation throughout May–July above 85 km.

## 6. Discussion

### 6.1. Wind Annual Climatology

In our study we have presented the first long-term radar wind observations from Antarctica made by a meteor radar with height resolving ability.

Here we consider comparisons between our radar observations and the WACCM-X predictions also presented in this work. We find that although there is agreement in some periods of the seasonal cycle, WACCM-X has persistent biases that occur every year. Specifically, in Antarctic winter at heights of 85–100 km, our radar observations reveal eastwards winds (of magnitude  $\sim 10 \text{ ms}^{-1}$ ) and yet WACCM-X predicts westwards winds (of magnitude  $\sim 5\text{--}10 \text{ ms}^{-1}$ ) that is, winds in the opposite direction. The observed and WACCM-X meridional wind results also differ in the summer at heights of 90–100 km. The radar observations reveal northwards winds ( $\sim 5\text{--}10 \text{ ms}^{-1}$ ) yet WACCM-X predicts southwards winds ( $\sim 10 \text{ ms}^{-1}$ ). This bias in the meridional winds has far reaching impacts in accurately modeling the chemical transport in the MLT and consequently the downwelling on chemical species at the poles.

In Zhou et al. (2022) they compare meteor radar wind observations in the MLT and SD-WACCM version 4 (note that whilst this is different from the WACCM-X version used in this paper, both versions are nudged to MERRA data) for a variety of low- and mid-latitude meteor radar sites in the Northern Hemisphere in China. Our meteor radar results show some similarity to the highest latitude site (Mohe,  $53.5^\circ\text{N}$ ,  $122.3^\circ\text{E}$ ) with the same summertime wind reversal appearing in the zonal winds. This suggests that the wintertime bias in zonal winds at high latitudes may also be present in the Northern Hemisphere. An important point to note here is that this bias is not present at the other lower latitude sites that they investigated.

Stober et al. (2021) carried out a comprehensive comparison of MLT winds from 6 meteor radar sites at conjugate latitudes with model results from WACCM-X, GAIA and UA-ICON (Borchert et al., 2019). They found the same summertime bias in the zonal winds between high latitude observations (in both hemispheres) and WACCM-X and UA-ICON, but not GAIA. They note that whilst WACCM-X and GAIA have similar gravity wave parametrization schemes, there are differences in the net zonal gravity wave drag and the vertical structure of this drag which could perhaps explain the differences (Stober et al., 2021). note that UA-ICON and WACCM-X parametrisations seem to be more appropriate for the summer mesopause wind reversal whereas GAIA is better for winter.

Dempsey et al. (2021) presented radar results from 2009 from Rothera and showed that both WACCM and eCMAM (the extended Canadian Middle Atmosphere Model) suffer from the same, westward (negative) winds in the winter as our results. Griffith et al. (2021) also finds very similar biases between ExUM (Extended Unified Model) and meteor radar winds at Rothera for 1 year. Our work extends on these single year studies and shows that the discrepancies are persistent biases occurring every year in our data set. Becker and Vadas (2018) propose that the missing eastwards gravity wave momentum in the models is responsible for this bias between observations and models of the wintertime winds. Their model, the HIAMCM (The High Altitude Mechanistic general Circulation Model) includes secondary gravity waves and correctly predicts the mesospheric wintertime eastward flow seen in the radar zonal climatology (Vadas et al., 2018). Neither WACCM-X (our study), WACCM and eCMAM (Dempsey et al., 2021) and the ExUM (Griffith et al., 2021) capture the winter eastwards winds above 85 km at Rothera. Our findings here are consistent with the hypothesis of Becker and Vadas, that secondary gravity wave processes are important in recreating the eastwards winds above 85 km found in the wintertime observations. More recently (Harvey et al., 2022), investigated this bias in further detail, finding that the modeled wintertime polar MLT zonal winds were closer in agreement to observations during periods where the polar night

jet below was weakened. This would allow the propagation of eastwards gravity waves into the MLT, driving winds that are more eastwards (in closer agreement with the observations). As proposed by Becker and Vadas (2018), they state that the lack of higher order waves in circulation models could be a reason for the bias. However they also discuss additional known deficiencies in the current gravity wave parametrization that could contribute to this bias. In their conclusions (Harvey et al., 2022), discuss future work to investigate this bias in more detail.

We can also make specific comparisons to other studies. Dowdy et al. (2007) presented climatologies of observations made by MF radars at Davis (69°S, 78°E, 1994–2005) and Syowa (69°S, 40°E, 1999–2003). Their zonal wind observations revealed some general similarities in the seasonal variability with our meteor radar results. However, there are notable differences. The MF radar observations of zonal winds show weaker eastwards winds above the zero wind line (5–10 ms<sup>-1</sup> in the MF radar winds compared to 10–20 ms<sup>-1</sup> in the meteor radar winds in January at heights of 95–100 km).

Baumgaertner et al. (2005) presented wind observations from 1985 to 2004 made by an MF radar (heights of 75–95 km) at Scott Base (78°S, 167°E). It is worth noting that the 10° latitude difference between Rothera and Scott Base may affect comparisons, however, due to the limited availability of Antarctic observations, this remains a useful comparison. In their study they found that there is a large degree of interannual variability in the wind speeds, noting that the interannual variability peaks in December zonal winds, in good general agreement with our results. We find that the climatologies presented by Baumgaertner et al. (2005) had much lower wind speeds in both zonal and meridional components, with the zonal summertime wind reversal reaching a maximum of 18 ms<sup>-1</sup> in their results compared with ~30 ms<sup>-1</sup> in our results. Additionally, although the data only extends to 95 km in height, the zero wind line in the zonal winds is higher in Baumgaertner et al. (2005) (95 km in January compared to 90 km in the meteor radar results) and the eastwards winds above are very weak. This is a similar difference to that seen when we compared our meteor radar to Dowdy et al. (2007).

Another study of interest is Hibbins et al. (2005), where wind observations for 1997–1998 and 2002–2004 from the MF radar at Rothera (i.e., the same location as our meteor radar) were presented. The average year presented by Hibbins et al. (2005) shows some general agreement with our average year from the meteor radar observed winds. However, the zero wind line in both the zonal and meridional winds is far lower in height in Hibbins et al. (2005) than our results in this work. For example, in January the zonal zero wind line is 6 km lower in Hibbins et al. (2005) and in June the meridional zero wind line is 8 km lower. As noted by Sandford et al. (2010) this is significantly different to both Antarctic MF and meteor radar climatologies and that later analysis of the Rothera MF-radar data from 2005 onwards shows a much higher summertime zero-wind line, closer to the results of other MF radar studies. We suggest that this may indicate a bias in height estimates in data from the Rothera MF radar recorded before 2005.

(Imura et al., 2011) also explored high latitude MF radar results in their paper comparing MF winds, semi-diurnal tides and diurnal tides over 1999–2010 for Syowa (69°S, 39.6°E) and Andenes (69.3°N, 16°E). The magnitude of observed winds at Syowa and our study are comparable and like our work, they also found significant interannual variability in observed winds. They compared their observations to (Sandford et al., 2010) which discussed the same meteor radar winds from Rothera as this study for 2005–2010 (Imura et al., 2011). noted that specific differences may be due to the longitudinal difference of the sites and the influence of stationary planetary waves.

In summary, we find that there are differences between our meteor radar observed winds and the MF radar winds from Baumgaertner et al. (2005), Dowdy et al. (2007) and Hibbins et al. (2009). These discrepancies may arise due to interannual variability, longitudinal differences or biases between the different techniques. Here, we draw attention to Manson et al. (2004) and Jacobi et al. (2009) where the differences between MF radar and meteor radar observed winds for collocated instruments were quantified. In general, although there is good agreement at heights of 80–90 km, MF radars were found to record significantly weaker winds at heights above 85–90 km than were recorded by meteor radars. Wilhelm et al. (2017) also explored the differences between the meteor radar and MF radar winds. They attribute the differences to two potential reasons, both arising from the MF radar technique. Firstly, differences between the measured centre of scatters and the true centre in the MF radar beam and secondly, sidelobe contamination. This highlights the suitability of MF radar studies for winds below 80 km and meteor radar for above 80 km.

## 6.2. Linear Regression Results

In this study we have regressed wind observations from the meteor radar and WACCM-X predictions against time and five climatological indices. As discussed in Section 3.1 we acknowledge that these are not the only possibly drivers of interannual variability and that the method assumes any relationships are linear. Due to our use of 3 month windows, there may be some intra-seasonal contamination in our results. Additionally, when comparing correlations between the indices in the winds in the observations and the model it is important to note that (particularly in winter in the zonal winds) the background winds do not agree. The results of our linear regression are discussed below.

### 6.2.1. Trends With Time

In any long term data set, an exploration into trends with time is vital. One of the main strengths of this study lies in the length of the data set (2005–2021). This is the longest such study from an Antarctic meteor radar with height finding capability. Even though 3 years are removed due to poor data quality, the range of this time period allows us to identify and separate long term trends from the influence of the 11-year solar cycle. This is something which Qian et al. (2019) notes can be very difficult in shorter studies. There have been a number of studies on long term trends in the MLT region. Beig et al. (2003) carried out a comprehensive review of long term temperature changes in the middle/upper atmosphere (heights of 50–100 km) and associated them with anthropogenic activities. They emphasized that increases in greenhouse gases are expected to have a substantial impact on the radiative-chemical-dynamical equilibrium of the middle atmosphere. More recently, longer observational data sets and model capabilities have allowed for further long term studies which are noted in the updated review, Beig (2011a). The review finds that for southern hemisphere temperatures in the MLT region, there is a cooling trend. However, they specifically highlight the importance of exploring different trends in different seasons, for example, French and Mulligan (2010) found that the cooling trend maximized in September/October, coincident with Antarctic ozone depletion. Ramesh et al. (2020) in a multi-linear regression study using WACCM 6 also finds a correlation between increased atmospheric CO<sub>2</sub> and a cooling throughout the whole upper atmosphere for June–August and December–February (they did not investigate other time periods).

There have been a few long term trend analyses using observational meteor radar wind data sets. Recently, Jaen et al. (2023), studied summertime trends using MF radars and meteor radars in Northern and middle latitudes. At northern high latitudes, they found a weakening of the eastwards winds at 90–105 km of 4.5 ms<sup>-1</sup> per decade which is in agreement with the results that we see in Figure 6a, where the hatched blue region at heights of 90–100 km throughout October to March indicate the eastwards winds have a more westwards trend (i.e., are weakening) at a rate of between 3 and 7 ms<sup>-1</sup> per decade. This suggests that the wind trends found in our study may have similarities to the northern hemisphere. They also found a strengthening of the westward wind jet in the mesosphere (centered around 70 km but reaching up to 90 km at times) at middle latitudes but no clear trend in northern latitudes, our results suggest a small strengthening of this westwards summertime jet around 80 km. Jacobi et al. (2012) carried out a piece-wise trend analysis on northern hemisphere midlatitude meteor radar sites. They found that wind trends varied by longitude, which they attribute to standing planetary wave influence. This location dependence highlights the complexity of observational analysis of wind trends in the MLT, especially with ground based radar. Wilhelm et al. (2019) in their study from three northern hemisphere meteor radars, found that the zonal and meridional wind at all three sites exhibited a linear trend in time in some seasons, although the pattern of this trend varied across all three sites. More recently, Song et al. (2023) carried out an exploration into trends and solar cycle influences for 2007–2021 using data from a meteor radar at King Sejong Station in Antarctica. They found conflicting trends to our findings in Antarctic summer, however, they also found a trend toward a strengthening of the eastwards winds in winter around 85–95 km which agrees with our results. All three meteor radar studies (Jacobi et al. (2012), Wilhelm et al. (2019) and Song et al. (2017)) use meteor radars with height finding capabilities and find varying trends at different heights, this height dependence is also present in our findings and emphasizes the importance of using meteor radars with height finding capability when exploring long term trends in the MLT region.

Using MF radar (Iimura et al., 2011) explored long term trends over 1999–2010 for Syowa (69°S, 39.6°E) and Andenes (69.3°N, 16°E). They found positive trends of up to 2 ms<sup>-1</sup> per year in winter around 70 km but stretching up to 95 km (the top of their data set) for August. They also found significant positive correlations

around 70–85 km in January–March of up to around  $1 \text{ ms}^{-1}$  per year. This equates to up to  $10 \text{ ms}^{-1}$  per decade and is similar in magnitude to the wind correlations we found in our results.

The seasonal dependence found throughout all the studies mentioned in this section is especially clear in our results presented in this paper. The majority of studies agree that there is a significant trend in the MLT for at least some times of the year. Despite the studies disagreeing in what this trend is (possibly due to variations in location and time period), it indicates that the MLT winds are experiencing a significant change with time. We note that these trends in the winds are found alongside significant cooling trends in the Southern Hemisphere MLT region as discussed by Beig (2011a) and associated with anthropogenic activity.

### 6.2.2. The 11 years Solar Cycle

In a companion paper to Beig (2011a) on long term trends, Beig (2011b) summarized studies of solar cycle influence on MLT temperatures, and found that a solar maximum increases temperatures by a few K per 100 solar flux units (sfu), and that this change increased to about (4–5 K per 100 sfu) at the upper heights of the MLT region. Later, a combined modeling and observational paper by Gan et al. (2017) found significant temperature responses in SABER (Sounding of the Atmosphere using Broadband Emission Radiometry), a satellite-based instrument and eCMAM (extended Canadian Middle Atmosphere Model) using a linear regression method. They found a significant correlation between solar maximum and a hotter atmosphere in the middle and upper atmosphere, with the temperature response increasing with height. This is in agreement with the temperature responses summarized by Beig (2011b) and found by Ramesh et al. (2020) and Cullens et al. (2016) using the WACCM model. The wind responses in Gan et al. (2017), Ramesh et al. (2020) and Cullens et al. (2016) are less statistically significant and more variable than the temperature response. This is perhaps due to the complex wave processes governing the winds in the MLT. However, all three studies find a significant relationship between the solar cycle and the Antarctic MLT winds, at least during some seasons. This is in general agreement with our results from observations, however, WACCM-X winds shows no correlation with the solar cycle in either wind direction.

We find the largest positive correlation with F10.7 in the observed zonal wind at heights of 80–98 km in spring and early summer, this correlation is found in the radar observations but not the WACCM-X predictions. We compare this to Ramesh et al. (2020) where WACCM6 temperature and wind results were regressed against indices for F10.7, QBO, ENSO, EESC (Equivalent Effective Stratospheric Chlorine),  $\text{CO}_2$  and AOD (area-weighted global average of stratospheric aerosol optical depth at 550 nm). We find that, for the latitude of Rothera, our result of a positive correlation of F10.7 with the zonal winds agrees with Ramesh et al. (2020). However, the response in Ramesh et al. (2020) is  $\sim 1 \text{ ms}^{-1}$  per 100 sfu, much smaller than the response of  $\sim 5$ – $8 \text{ ms}^{-1}$  per 100 sfu found in our results. A possible reason for this magnitude difference could be the time period used: Ramesh et al. (2020) used a much longer interval (1850–2014) and it is recognised that trend results can be dependent on the time period Beig (2011a). Additionally, Ramesh et al. (2020) considered zonal-mean zonal-winds, whilst our radar and analysis of WACCM-X data are localized to the zonal winds at Rothera. Smith (2012) states that due to planetary scale oscillations in monthly averaged winds, the local time-averaged zonal wind is likely to differ from the zonal-mean zonal-wind.

Cullens et al. (2016) also used WACCM to explore the influence of the solar cycle on temperature and wind in the atmosphere. Cullens et al. (2016), like Ramesh et al. (2020) used zonal-mean zonal-wind values. For the latitude of Rothera, our results disagree with those from Cullens et al. (2016) who found that the winds are significantly more westwards during a solar maximum than a solar minimum during September–October and with no significant change in December–January. We propose that our WACCM-X results differ to that of Cullens et al. (2016) due to the different time periods analyzed. Cullens et al. (2016) used model data for 1955–2005; not only is this a far longer period, incorporating 5 solar maxima, it has no overlap with our study.

Baumgaertner et al. (2005) examined observational wind data from 1985 to 2004 from an MF radar at Scott Base, Antarctica. They found no significant correlation between the solar cycle and winds (when partitioning for QBO phase); however, this station is significantly further poleward than Rothera. Wilhelm et al. (2019) fitted an 11-year period sine wave (unconstrained in phase) to radar winds from three northern hemisphere sites in the Arctic. Andenes at ( $69^\circ\text{N}$ ,  $16^\circ\text{E}$ ) is at conjugate latitudes to Rothera and Wilhelm et al. (2019) found the strongest amplitude response in summer ( $2$ – $4 \text{ ms}^{-1}$  at heights of 80–85 km in June–August). This is in general agreement with our results from the meteor radar and suggests that similar correlations in observed



winds with the solar cycle may be evident in both the Arctic and Antarctic, although differences in methodology preclude further comparisons in the sign of this correlation. In the meridional component Wilhelm et al. (2019) found little significant change in the winds with the 11-year solar cycle, this is in broad agreement with our radar results where there were no persistent statistically significant correlations with the solar cycle.

### 6.2.3. The El Niño Southern Oscillation

In the radar observations for the regression results from the ENSO coefficient, there are no regions of statistically significant correlations aside from in May. This leads us to conclude that there is little linear influence on the MLT winds by ENSO throughout the year, except for May. Li et al. (2016) explore the response of the summer southern hemisphere MLT winds to ENSO, proposing a mechanism wherein Northern Hemisphere planetary wave activity is increased during an El Niño event causing a chain of changes leading to anomalous southern hemisphere mesospheric eastward gravity wave forcing at heights of 70–100 km. Llamedo et al. (2019) also found a 3.5–4 years oscillation in lidar observed gravity wave activity in the stratosphere in Tierra del Fuego that they suggest could be an ENSO influence. Ramesh et al. (2020) found that the zonal mean winds have the strongest and geographically largest regions of correlation to ENSO at mid latitudes. Whereas at higher latitudes, the correlation is weaker but still significant at times. We see in our radar results the strongest response in May, however, Ramesh et al. (2020) does not present results for May and so we are unable to compare. Our results suggest that there may be some interaction between ENSO and the MLT winds during May but not throughout the rest of the year.

For the results from WACCM-X there is no significant correlation between the winds and ENSO, suggesting no such relationship between this index and the winds in the model.

### 6.2.4. The Quasi-Biennial Oscillation

For the QBO results there is little agreement between the radar results and the WACCM-X. The wind responses to the QBO10 and QBO30 index also show no notable similarities with each other as expected because the indices are orthogonal. Ramesh et al. (2020) also used a QBO10 and QBO30 term in their linear regression analysis of WACCM6 zonal mean zonal winds. Their results showed the QBO response as a primarily equatorial response that did not extend above the stratopause throughout June–August. In their results for the MLT region, in December–February the QBO has an influence on the equatorial region and the northern hemisphere, but not the southern hemisphere. Ford et al. (2009) explored the QBO effects on Antarctic mesospheric winds using an Imaging Doppler Interferometer at Halley (75.6°S, 25.5°W) and found that different lags of the QBO at 50 hPa correlated with wind effects at different times of the year in the mesosphere. They proposed that the winds are modulated by action of the equatorial QBO on planetary wave activity. We see little agreement when comparing the results with Ford et al. (2009) at nearly similar QBO pressure levels; at 7 hPa (34 km) to our 10 hPa (31 km) and the 23 hPa (27 km) to 30 hPa (24 km). However, this may be a product of the different time periods used, different location or different observational techniques. In contrast, using MF radar winds from Scott Base, Antarctica, Baumgaertner et al. (2005) found no consistent relationship between MLT winds and the QBO using a variety of techniques.

Like Ford et al. (2009), our regression results show that there is a significant influence from the QBO on the Antarctic MLT at some times of the year. This could be due to the differential filtering of gravity waves through the alternating wind directions of the QBO and the importance of wave driving for MLT dynamics. However, the full complex influence of the QBO on MLT winds is hard to characterize by only considering the two indices. In this study, the inclusion of the QBO10 and QBO30 indices serve to identify that there is a change in the winds during times of opposing QBO phases and to remove the main effects of the QBO from the other results. More research is needed to understand the processes behind this link between the QBO winds and the Antarctic MLT dynamics.

### 6.2.5. The Southern Annular Mode

There have been very few previous studies on the influence of the SAM on Antarctic MLT winds. Merzlyakov et al. (2009) found no significant correlations between the winter zonal wind and the SAM index with a composite data set of radar observations (with no height resolving ability) for 1970 to 2006 across a variety of Antarctic sites.

This is consistent with our radar observations where there is little significant influence of the SAM on the zonal winds in winter (as per Figure 6k). However, in winter WACCM-X results there is a strong, significant positive correlation between the zonal winds and the SAM index that is not present in observations.

In summer, from observations, we see a large negative correlation between the zonal wind and the SAM index. A possible suggestion for this is in the influence of the SAM on filtering gravity wave propagation from the surface. In the meridional direction there is little significant correlation suggesting that MLT wind correlations with the SAM are primarily zonal.

## 7. Conclusions

In this work we have carried out the first long-term study of the seasonal and interannual variability of Antarctic MLT winds using the meteor radar at Rothera on the Antarctic Peninsula. We have presented a multi-year climatology of meridional and zonal winds and compared these meteor radar observations to predictions from WACCM-X. Further, we have characterized the interannual variability of both observed and modeled winds with a multilinear regression model, regressing against six key indices, namely; time, the 11-year solar cycle, El Niño Southern Oscillation (ENSO), two indices for the Quasi-Biennial Oscillation (QBO) and the Southern Annular Mode (SAM). We find that there are notable differences between the observed and modeled winds in both the multi-year seasonal climatology and in their interannual variation with climatological indices.

From our work, we conclude that.

1. Persistent biases are found between observations and the WACCM-X model. In particular, the observations reveal *eastward* winds of  $\sim 10 \text{ ms}^{-1}$  in wintertime (April–September) at heights from about 85 to 100 km, but at these heights WACCM-X predicts *westward* winds of  $\sim 5\text{--}10 \text{ ms}^{-1}$ . In the meridional component, summertime (October–March inclusive) winds at heights from 80 to 100 km are observed to be *northwards* but are predicted to be *southwards* from 90 to 100 km in WACCM-X.
2. Both the observed and model winds show a significant degree of interannual variability with the highest interdecile range occurring between September–December in the zonal winds, largely due to variations in the strength and height of the summertime wind reversal.
3. The summertime westwards winds near 80 km are weakening by up to  $5 \text{ ms}^{-1}$  per decade, with the eastwards winds above this also weakening throughout summer. Simultaneously, the eastward wintertime winds around 85–95 km are also strengthening by up to  $5 \text{ ms}^{-1}$  per decade. However, none of these changes are reflected in WACCM-X. This seasonal structure in the trends highlights the importance of partitioning by season and height when examining data for long term trends.
4. In summer (October–March inclusive), the observed zonal winds vary with the solar cycle. In particular, at heights of 80–95 km these winds are up to  $9 \text{ ms}^{-1}$  more eastwards for an increase in solar activity of 100 sfu. WACCM-X has no such correlation.
5. The variation of observed wind with the Niño3.4 ENSO index is sporadic and generally less significant than for the other indices, however we see a small correlation throughout May–June above 90 km between the observed wind and ENSO. This suggests that for the majority of the year, there is no clear linear ENSO influence on the MLT Antarctic winds. No correlation between the model winds and ENSO is found.
6. Determining the wind response to the QBO is challenging with a linear regression method due to the characteristic descending phases of eastwards and westwards winds and their role in the filtering of gravity waves. In our results, we find differing responses to the QBO between the observations and the model and depending on the height used to capture the QBO behavior.
7. The relationship between MLT winds and the SAM has not previously been explored in detail in other studies. Our results suggest that both the observed and model MLT zonal winds do vary strongly and significantly with SAM. However, the sign and timing of this response differs between the observations and WACCM-X. This may be a consequence of filtering of gravity waves by the SAM.

This work highlights the importance of using observations to constrain GCMs as they are extended upwards into the mesosphere and above.

### Data Availability Statement

Data for F10.7 is provided by (Government of Canada, 2022). Data for ENSO comes from Nino 3.4 index, Trenberth (2022). QBO indices from ERA5 reanalysis, Copernicus Climate Change Service (2022), and the SAM from Marshall (2018). The meteor radar data used in this work is from Mitchell (2021). The WACCM-X data is available alongside the code and processed meteor radar data at Noble (2023).

### Acknowledgments

PN is supported by a NERC GW4+ Doctoral Training Partnership studentship from the Natural Environment Research Council (NE/S007504/1). CW, NH, NM and TMG are supported by the UK Natural Environment Research Council (NERC) under Grants NE/R001391/1, NE/S00985X/1 and NE/R001235/1. CW is also supported by a Royal Society University Research Fellowship URF/R/221023 and NH is also supported by a NERC independent fellowship NE/X017842/1. CYC is supported by NSF 1855476. This material is based upon work supported by the National Center for Atmospheric Research, which is a major facility sponsored by the U.S. National Science Foundation under Co-operative Agreement 1852977. NP acknowledges support from NASA Grant 80NSSC20K0628.

### References

Baumgaertner, A., McDonald, A., Fraser, G., & Plank, G. (2005). Long-term observations of mean winds and tides in the upper mesosphere and lower thermosphere above Scott base, Antarctica. *Journal of Atmospheric and Solar-Terrestrial Physics*, 67(16), 1480–1496. <https://doi.org/10.1016/j.jastp.2005.07.018>

Becker, E., & Vadas, S. L. (2018). Secondary gravity waves in the winter mesosphere: Results from a high-resolution global circulation model. *Journal of Geophysical Research: Atmospheres*, 123(5), 2605–2627. <https://doi.org/10.1002/2017JD027460>

Beig, G. (2011). Long-term trends in the temperature of the mesosphere/lower thermosphere region: 1. Anthropogenic influences. *Journal of Geophysical Research*, 116(A2). <https://doi.org/10.1029/2011JA016646>

Beig, G. (2011). Long-term trends in the temperature of the mesosphere/lower thermosphere region: 2. Solar response. *Journal of Geophysical Research*, 116(A2). <https://doi.org/10.1029/2011JA016766>

Beig, G., Keckhut, P., Lowe, R. P., Roble, R., Mlynczak, M., Scheer, J., et al. (2003). Review of mesospheric temperature trends. *Reviews of Geophysics*, 41(4). <https://doi.org/10.1029/2002rg000121>

Bojkov, R. D., & Fioletov, V. E. (1995). Estimating the global ozone characteristics during the last 30 years. *Journal of Geophysical Research*, 100(D8), 16537–16551. <https://doi.org/10.1029/95JD00692>

Borchert, S., Zhou, G., Baldauf, M., Schmidt, H., Zängl, G., & Reinert, D. (2019). The upper-atmosphere extension of the icon general circulation model (version: Ua-icon-1.0). *Geoscientific Model Development*, 12(8), 3541–3569. <https://doi.org/10.5194/gmd-12-3541-2019>

Bremer, J., Schindler, R., Greisiger, K., Hoffmann, P., Kürschner, D., & Singer, W. (1997). Solar cycle dependence and long-term trends in the wind field of the mesosphere/lower thermosphere. *Journal of Atmospheric and Solar-Terrestrial Physics*, 59(5), 497–509. [https://doi.org/10.1016/s1364-6826\(96\)00032-6](https://doi.org/10.1016/s1364-6826(96)00032-6)

Cai, B., Xu, Q., Hu, X., Cheng, X., Yang, J., & Li, W. (2021). Analysis of the correlation between horizontal wind and 11-year solar activity over Langfang, China. *Earth and Planetary Physics*, 5(3), 270–279. <https://doi.org/10.26464/epp2021029>

Chiodo, G., Marsh, D. R., Garcia-Herrera, R., Calvo, N., & Garcia, J. A. (2014). On the detection of the solar signal in the tropical stratosphere. *Atmospheric Chemistry and Physics*, 14(11), 5251–5269. <https://doi.org/10.5194/acp-14-5251-2014>

Copernicus Climate Change Service. (2022). Era5 hourly data on pressure levels from 1940 to present. [dataset]. <https://doi.org/10.24381/cds.bd0915c6>

Cullens, C. Y., England, S. L., & Garcia, R. R. (2016). The 11 year solar cycle signature on wave-driven dynamics in waccm. *Journal of Geophysical Research: Space Physics*, 121(4), 3484–3496. <https://doi.org/10.1002/2016ja022455>

Dempsey, S. M., Hindley, N. P., Moffat-Griffin, T., Wright, C. J., Smith, A. K., Du, J., & Mitchell, N. J. (2021). Winds and tides of the Antarctic mesosphere and lower thermosphere: One year of meteor-radar observations over Rothera (68s, 68w) and comparisons with WACCM and eCMAM. *Journal of Atmospheric and Solar-Terrestrial Physics*, 212, 105510. <https://doi.org/10.1016/j.jastp.2020.105510>

Dowdy, A. J., Vincent, R. A., Tsutsumi, M., Igarashi, K., Murayama, Y., Singer, W., & Murphy, D. J. (2007). Polar mesosphere and lower thermosphere dynamics: 1. Mean wind and gravity wave climatologies. *Journal of Geophysical Research*, 112(D17). <https://doi.org/10.1029/2006JD008126>

Field, A. (2013). *Discovering statistics using IBM SPSS statistics*. sage.

Ford, E. A. K., Hibbins, R. E., & Jarvis, M. J. (2009). QBO effects on Antarctic mesospheric winds and polar vortex dynamics. *Geophysical Research Letters*, 36(20). <https://doi.org/10.1029/2009GL039848>

French, W. J. R., Klekociuk, A. R., & Mulligan, F. J. (2020). Analysis of 24 years of mesopause region oh rotational temperature observations at Davis, Antarctica—part 1: Long-term trends. *Atmospheric Chemistry and Physics*, 20(11), 6379–6394. <https://doi.org/10.5194/acp-20-6379-2020>

French, W. J. R., Klekociuk, A. R., & Mulligan, F. J. (2020b). Analysis of 24 years of mesopause region oh rotational temperature observations at Davis, Antarctica—part 2: Evidence of a quasi-quadrennial oscillation (QO) in the polar mesosphere. *Atmospheric Chemistry and Physics*, 20(14), 8691–8708. <https://doi.org/10.5194/acp-20-8691-2020>

French, W. J. R., & Mulligan, F. J. (2010). Stability of temperatures from timed/saber v1. 07 (2002–2009) and AURA/MLS v2. 2 (2004–2009) compared with oh (6–2) temperatures observed at Davis station, Antarctica. *Atmospheric Chemistry and Physics*, 10(23), 11439–11446. <https://doi.org/10.5194/acp-10-11439-2010>

Fritts, D. C., & Alexander, M. J. (2003). Gravity wave dynamics and effects in the middle atmosphere. *Reviews of Geophysics*, 41(1), 1003. <https://doi.org/10.1029/2001RG000106>

Gan, Q., Du, J., Fomichev, V. I., Ward, W. E., Beagley, S. R., Zhang, S., & Yue, J. (2017). Temperature responses to the 11 year solar cycle in the mesosphere from the 31 year (1979–2010) extended Canadian middle atmosphere model simulations and a comparison with the 14 year (2002–2015) timed/saber observations. *Journal of Geophysical Research: Space Physics*, 122(4), 4801–4818. <https://doi.org/10.1002/2016ja023564>

Gareth, J., Daniela, W., Trevor, H., & Robert, T. (2013). *An introduction to statistical learning: With applications in r*. Springer.

Gillett, N. P., Kell, T. D., & Jones, P. D. (2006). Regional climate impacts of the southern annular mode. *Geophysical Research Letters*, 33(23). <https://doi.org/10.1029/2006GL027721>

Government of Canada, N. R. C. (2022). F10.7. [dataset]. National Research Council of Canada, Government of Canada / Gouvernement du Canada. Retrieved from <https://www.spaceweather.ca/forecast-prevision/solar-solaire/solarflux/sx-en.php>

Greisiger, K., Schindler, R., & Kürschner, D. (1987). Long-period variations of wind parameters in the mesopause region and the solar cycle dependence. *Journal of Atmospheric and Terrestrial Physics*, 49(3), 281–285. [https://doi.org/10.1016/0021-9169\(87\)90063-8](https://doi.org/10.1016/0021-9169(87)90063-8)

Griffith, M. J., Dempsey, S. M., Jackson, D. R., Moffat-Griffin, T., & Mitchell, N. J. (2021). Winds and tides of the extended unified model in the mesosphere and lower thermosphere validated with meteor radar observations. *Annales Geophysicae*, 39(3), 487–514. <https://doi.org/10.5194/angeo-39-487-2021>

Harvey, V. L., Pedatella, N., Becker, E., & Randall, C. (2022). Evaluation of polar winter mesopause wind in waccmx+dart. *Journal of Geophysical Research: Atmospheres*, 127(15), e2022JD037063. <https://doi.org/10.1029/2022JD037063>

- Hibbins, R. E., Jarvis, M., & Ford, E. (2009). Quasi-biennial oscillation influence on long-period planetary waves in the Antarctic upper mesosphere. *Journal of Geophysical Research*, *114*(D9). <https://doi.org/10.1029/2008jd011174>
- Hibbins, R. E., Shanklin, J. D., Espy, P. J., Jarvis, M. J., Riggins, D. M., Fritts, D. C., & Lübken, F.-J. (2005). Seasonal variations in the horizontal wind structure from 0–100 km above Rothera station, Antarctica (67°S, 68°W). *Atmospheric Chemistry and Physics*, *5*(11), 2973–2980. <https://doi.org/10.5194/acp-5-2973-2005>
- Hindley, N. P., Mitchell, N. J., Cobbett, N., Smith, A. K., Fritts, D. C., Janches, D., et al. (2022). Radar observations of winds, waves and tides in the mesosphere and lower thermosphere over South Georgia island (54°S, 36°W) and comparison with WACCM simulations. *Atmospheric Chemistry and Physics*, *22*(14), 9435–9459. <https://doi.org/10.5194/acp-22-9435-2022>
- Hocking, W., Fuller, B., & Vandeeper, B. (2001). Real-time determination of meteor-related parameters utilizing modern digital technology. *Journal of Atmospheric and Solar-Terrestrial Physics*, *63*(2–3), 155–169. [https://doi.org/10.1016/s1364-6826\(00\)00138-3](https://doi.org/10.1016/s1364-6826(00)00138-3)
- Hoffmann, L., Xue, X., & Alexander, M. J. (2013). A global view of stratospheric gravity wave hotspots located with Atmospheric Infrared Sounder observations. *Journal of Geophysical Research*, *118*(2), 416–434. <https://doi.org/10.1029/2012JD018658>
- Imura, H., Fritts, D. C., Tsutsumi, M., Nakamura, T., Hoffmann, P., & Singer, W. (2011). Long-term observations of the wind field in the Antarctic and Arctic mesosphere and lower-thermosphere at conjugate latitudes. *Journal of Geophysical Research*, *116*(D20), D20112. <https://doi.org/10.1029/2011JD016003>
- Jacobi, C., Arras, C., Kürschner, D., Singer, W., Hoffmann, P., & Keuer, D. (2009). Comparison of mesopause region meteor radar winds, medium frequency radar winds and low frequency drifts over Germany. *Advances in Space Research*, *43*(2), 247–252. <https://doi.org/10.1016/j.asr.2008.05.009>
- Jacobi, C., Hoffmann, P., Liu, R., Merzlyakov, E., Portnyagin, Y. I., Manson, A., & Meek, C. (2012). Long-term trends, their changes, and interannual variability of northern hemisphere midlatitude MLT winds. *Journal of Atmospheric and Solar-Terrestrial Physics*, *75*, 81–91. <https://doi.org/10.1016/j.jastp.2011.03.016>
- Jacobi, C., Schminder, R., Kürschner, D., Bremer, J., Greisiger, K., Hoffmann, P., & Singer, W. (1997). Long-term trends in the mesopause wind field obtained from LF D1 wind measurements at COLLM, Germany. *Advances in Space Research*, *20*(11), 2085–2088. [https://doi.org/10.1016/S0273-1177\(97\)00599-1](https://doi.org/10.1016/S0273-1177(97)00599-1)
- Jaen, J., Renkwitz, T., Liu, H., Jacobi, C., Wing, R., Kuchař, A., et al. (2023). Long-term studies of the summer wind in the mesosphere and lower thermosphere at middle and high latitudes. *EGU sphere*, 1–21. <https://doi.org/10.5194/egusphere-2023-1465>
- Karlsson, B., & Kuilman, M. (2018). On how the middle atmospheric residual circulation responds to the solar cycle close to the Solstices. *Journal of Climate*, *31*(1), 401–421. <https://doi.org/10.1175/jcli-d-17-0202.1>
- Kishore, P., Venkat Ratnam, M., Velicogna, I., Sivakumar, V., Bencherif, H., Clemesha, B. R., et al. (2014). Long-term trends observed in the middle atmosphere temperatures using ground based lidars and satellite borne measurements. *Annales Geophysicae*, *32*(3), 301–317. <https://doi.org/10.5194/angeo-32-301-2014>
- Kutner, M. H., Nachtsheim, C. J., Neter, J., & Li, W. (2005). *Applied linear statistical models*. McGraw-Hill.
- Li, T., Calvo, N., Yue, J., Russell, J. M., Smith, A. K., Mlynczak, M. G., et al. (2016). Southern hemisphere summer mesopause responses to El Niño–Southern Oscillation. *Journal of Climate*, *29*(17), 6319–6328. <https://doi.org/10.1175/jcli-d-15-0816.1>
- Lindzen, R. S. (1981). Turbulence and stress owing to gravity wave and tidal breakdown. *Journal of Geophysical Research*, *86*(C10), 9707–9714. <https://doi.org/10.1029/jc086ic10p09707>
- Liu, H.-L., Bardeen, C. G., Foster, B. T., Lauritzen, P., Liu, J., Lu, G., et al. (2018). Development and validation of the whole atmosphere community climate model with thermosphere and ionosphere extension (WACCM-X 2.0). *Journal of Advances in Modeling Earth Systems*, *10*(2), 381–402. <https://doi.org/10.1002/2017MS001232>
- Llamedo, P., de la Torre, A., Alexander, P., Luna, D., Schmidt, T., & Wickert, J. (2009). A gravity wave analysis near to the Andes range from GPS radio occultation data and mesoscale numerical simulations: Two case studies. *Advances in Space Research*, *44*(4), 494–500. <https://doi.org/10.1016/j.asr.2009.04.023>
- Llamedo, P., Salvador, J., de la Torre, A., Quiroga, J., Alexander, P., Hierro, R., et al. (2019). 11 years of Rayleigh lidar observations of gravity wave activity above the southern tip of south America. *Journal of Geophysical Research: Atmospheres*, *124*(2), 451–467. <https://doi.org/10.1029/2018JD028673>
- Manson, A. H., Meek, C. E., Hall, C. M., Nozawa, S., Mitchell, N. J., Pancheva, D., et al. (2004). Mesopause dynamics from the Scandinavian triangle of radars within the PSMOS-DATAR project. *Annales Geophysicae*, *22*(2), 367–386. <https://doi.org/10.5194/angeo-22-367-2004>
- Marsh, D. R., Mills, M. J., Kinnison, D. E., Lamarque, J.-F., Calvo, N., & Polvani, L. M. (2013). Climate change from 1850 to 2005 simulated in CESM1(WACCM). *Journal of Climate*, *26*(19), 7372–7391. <https://doi.org/10.1175/jcli-d-12-00558.1>
- Marshall, G. (2003). Trends in the southern annular mode from observations and reanalyses. *Journal of Climate*, *16*(24), 4134–4143. [https://doi.org/10.1175/1520-0442\(2003\)016<4134:titsam>2.0.co;2](https://doi.org/10.1175/1520-0442(2003)016<4134:titsam>2.0.co;2)
- Marshall, G. (2018). The climate data guide: Marshall southern annular mode (sam) index (station-based). [dataset]. Retrieved from <https://climatedataguide.ucar.edu/climate-data/marshall-southern-annular-mode-sam-index-station-based>
- Merzlyakov, E., Murphy, D., Vincent, R., & Portnyagin, Y. (2009). Long-term tendencies in the MLT prevailing winds and tides over Antarctica as observed by radars at Molodezhnaya, Mawson and Davis. *Journal of Atmospheric and Solar-Terrestrial Physics*, *71*(1), 21–32. <https://doi.org/10.1016/j.jastp.2008.09.024>
- Middleton, H. R., Mitchell, N. J., & Muller, H. G. (2002). Mean winds of the mesosphere and lower thermosphere at 52°N in the period 1988–2000. *Annales Geophysicae*, *20*(1), 81–91. <https://doi.org/10.5194/angeo-20-81-2002>
- Mitchell, N. (2021). University of bath: Rothera skiyomet meteor radar data—Catalogue.ceda.ac.UK. [dataset]. Retrieved from <https://catalogue.ceda.ac.uk/uuid/20119725d15f40c39995a1787b67a94b>
- Montgomery, D. C. (2012). *Introduction to linear regression analysis*. Wiley.
- Nair, P. J., Godin-Beekmann, S., Kuttippurath, J., Ancellet, G., Goutail, F., Pazmiño, A., et al. (2013). Ozone trends derived from the total column and vertical profiles at a northern mid-latitude station. *Atmospheric Chemistry and Physics*, *13*(20), 10373–10384. <https://doi.org/10.5194/acp-13-10373-2013>
- Neale, R. B., Richter, J., Park, S., Lauritzen, P. H., Vavrus, S. J., Rasch, P. J., & Zhang, M. (2013). The mean climate of the community atmosphere model (CAM4) in forced SST and fully coupled experiments. *Journal of Climate*, *26*(14), 5150–5168. <https://doi.org/10.1175/jcli-d-12-00236.1>
- Noble, P. E. (2023). Seasonal-and-interannual-variability-of-winds-in-the-antarctic-mesosphere-and-lower-thermosphere: v2.1 [code]. Zenodo. <https://doi.org/10.5281/ZENODO.8224013>
- Portnyagin, Y., Forbes, J., Fraser, G., Vincent, R., Lysenko, I., & Makarov, N. (1992). Dynamics of the Antarctic and Arctic mesosphere/lower thermosphere regions. *Advances in Space Research*, *12*(10), 89–96. [https://doi.org/10.1016/0273-1177\(92\)90449-8](https://doi.org/10.1016/0273-1177(92)90449-8)

- Qian, L., Jacobi, C., & McInerney, J. (2019). Trends and solar irradiance effects in the mesosphere. *Journal of Geophysical Research: Space Physics*, *124*(2), 1343–1360. <https://doi.org/10.1029/2018JA026367>
- Ramesh, K., Smith, A. K., Garcia, R. R., Marsh, D. R., Sridharan, S., & Kishore Kumar, K. (2020). Long-term variability and tendencies in middle atmosphere temperature and zonal wind from WACCM6 simulations during 1850–2014. *Journal of Geophysical Research: Atmospheres*, *125*(24), e2020JD033579. <https://doi.org/10.1029/2020jd033579>
- Richter, J. H., Sassi, F., & Garcia, R. R. (2010). Toward a physically based gravity wave source parameterization in a general circulation model. *Journal of the Atmospheric Sciences*, *67*(1), 136–156. <https://doi.org/10.1175/2009JAS3112.1>
- Sandford, D. J., Beldon, C. L., Hibbins, R. E., & Mitchell, N. J. (2010). Dynamics of the Antarctic and Arctic mesosphere and lower thermosphere—Part 1: Mean winds. *Atmospheric Chemistry and Physics*, *10*(21), 10273–10289. <https://doi.org/10.5194/acp-10-10273-2010>
- Smith, A. K. (2012). Global dynamics of the MLT. *Surveys in Geophysics*, *33*(6), 1177–1230. <https://doi.org/10.1007/s10712-012-9196-9>
- Sofroniou, N., & Hutcheson, G. D. (1999). The multivariate social scientist. *The Multivariate Social Scientist*, 1–288.
- Song, B. G., Chun, H.-Y., Song, I.-S., Lee, C., Kim, J.-H., & Jee, G. (2023). Long-term characteristics of the meteor radar winds observed at King Sejong station, Antarctica. *Journal of Geophysical Research: Atmospheres*, *128*(1), e2022JD037190. <https://doi.org/10.1029/2022jd037190>
- Song, I. S., Lee, C., Kim, J. H., Jee, G., Kim, Y. H., Choi, H. J., et al. (2017). Meteor radar observations of vertically propagating low-frequency inertia-gravity waves near the southern polar mesopause region. *JGR*, *122*(4), 4777–4800. <https://doi.org/10.1002/2016JA022978>
- Stober, G., Kuchar, A., Pokhotelov, D., Liu, H., Liu, H.-L., Schmidt, H., et al. (2021). Interhemispheric differences of mesosphere–lower thermosphere winds and tides investigated from three whole-atmosphere models and meteor radar observations. *Atmospheric Chemistry and Physics*, *21*(18), 13855–13902. <https://doi.org/10.5194/acp-21-13855-2021>
- Sundararajan, S. (2020). Equatorial upper mesospheric mean winds and tidal response to strong El Niño and La Niña. *Journal of Atmospheric and Solar-Terrestrial Physics*, *202*, 105270. <https://doi.org/10.1016/j.jastp.2020.105270>
- Trenberth, K. N. (2022). Nino SST indices. [dataset]. Retrieved from <https://climatedataguide.ucar.edu/climate-data/nino-sst-indices-nino-12-3-34-4-oni-and-tni>
- Vadas, S. L., Zhao, J., Chu, X., & Becker, E. (2018). The excitation of secondary gravity waves from local body forces: Theory and observation. *Journal of Geophysical Research: Atmospheres*, *123*(17), 9296–9325. <https://doi.org/10.1029/2017JD027970>
- Webster, A. (2012). *Introductory regression analysis: With computer application for business and economics*. Taylor & Francis Group.
- Wilhelm, S., Stober, G., & Brown, P. (2019). Climatologies and long-term changes in mesospheric wind and wave measurements based on radar observations at high and mid latitudes. *Annales Geophysicae*, *37*(5), 851–875. <https://doi.org/10.5194/angeo-37-851-2019>
- Wilhelm, S., Stober, G., & Chau, J. L. (2017). A comparison of 11-year mesospheric and lower thermospheric winds determined by meteor and MF radar at 69°N. *Annales Geophysicae*, *35*(4), 893–906. <https://doi.org/10.5194/angeo-35-893-2017>
- Zhou, B., Xue, X., Yi, W., Ye, H., Zeng, J., Chen, J., & Dou, X. (2022). A comparison of MLT wind between meteor radar chain data and SD-WACCM results. *Earth and Planetary Physics*, *6*(5), 451–464.